J|A|C|S
ARTICLES
Published on Web 05/22/2003

Solid State Separated-Local-Field NMR Spectroscopy on Half-Integer Quadrupolar Nuclei: Principles and Applications to Borane Analysis

Julia Grinshtein and Lucio Frydman*

Contribution from the Department of Chemical Physics, Weizmann Institute of Sciences, 76100 Rehovot, Israel

Received December 2, 2002; E-mail: lucio.frydman@weizmann.ac.il

Abstract: New multidimensional NMR methods correlating the quadrupolar and heteronuclear dipolar interactions affecting a half-integer quadrupolar spin in the solid state are introduced and exemplified. The methods extend separated-local-field magic-angle spinning (SLF MAS) NMR techniques that have been used successfully in spin-$^1/_2$ spectroscopy to the study of $S \geq {}^3/_2$ nuclei. In our implementation, these techniques avoid homonuclear proton decoupling requirements by relying on moderately fast MAS rates (6−15 kHz) and use rotor-synchronized constant-time pulse sequences to achieve nearly arbitrary amplifications of the apparent dipolar coupling strengths. The result is a suite of simple 2D NMR experiments, whose line shapes carry valuable information about the structure and dynamics of solids containing quadrupolar and proton nuclei. The potential of these sequences was exploited to gather new insight into the structure and dynamics of a variety of boron-containing samples. These experimental SLF schemes were also extended to 3D NMR experiments that incorporate multiple-quantum MAS, thus enabling the resolution needed to study multiple chemical sites in a solid and providing a useful tool for the assignment of inequivalent sites.

Introduction

Over two-thirds of NMR-active, stable nuclei possess a noninteger spin with a quadrupole moment ($S = {}^3/_2, {}^5/_2$...). These nuclei partake in a majority of inorganic, organic, and biological structures, and therefore, their NMR characterization has long been a major focus of study.[1−5] NMR analyses of these nuclei in solids are complicated by the strong and anisotropic nature of the quadrupole interaction that affects them. Among the various NMR transitions allowed in these spins, however, quadrupole effects will leave unaffected to first order the central $-{}^1/_2 \leftrightarrow +{}^1/_2$ one. This feature has made central-transition NMR spectroscopy a method of choice for the study of this kind of nuclei. Still, quadrupole interactions can be sufficiently strong to warrant consideration of higher-order quadrupolar effects, which will often broaden central-transition NMR spectra when investigating powdered samples. Powder line shapes will even be observed when studying such system under the action of magic-angle spinning (MAS),[6,7] an approach which though normally successful for averaging first-order dipolar or chemical shift anisotropies will only reduce partially the broadening arising from second-order quadrupolar effects.[3−5,8−10]

Despite these resolution limitations, central-transition spectroscopy is one of the most common routes to study inorganic and bioinorganic solids by NMR. If sufficiently resolved, quadrupole line shapes can be fitted to extract the principal components of the electric field gradient tensors.[11,12] Yet even in this best-case scenario, translating this tensorial information into a picture of the local nuclear environments is not a trivial task. Despite the considerable progress made in the area of estimating and computing field gradients from quantum mechanical principles, the complexity associated with solid lattices hinders a one-to-one translation of quadrupole couplings into chemical structures. An important aid in helping to define the microstructure of a quadrupolar site could come from invoking other interactions, like the heteronuclear dipole−dipole coupling. By contrast to the quadrupole interaction, this coupling has a well-understood origin and a straightforward structural dependence, a feature that has made dipolar couplings the observables of choice when attempting to retrieve structural information from organic and biological solids.[13−16] Among the earliest ap-

(1) Cohen, M. H.; Reif, F. *Solid State Phys.* **1957**, *5*, 321.
(2) Abragam, A. *Principles of Nuclear Magnetism*; Oxford University Press: New York, 1961.
(3) Anderson, M. W., Duer, M. J., Eds. New NMR Techniques for Quadrupolar Nuclei. *Solid State NMR* **1999**, *15*.
(4) Fitzgerald, J., Ed. *Solid State NMR of Inorganic Materials*; ACS Symposium Series 717; American Chemical Society: Washington, DC, 1999.
(5) Smith, M. E.; vanEck, E. R. H. *Prog. NMR Spectroscopy* **1999**, *34*, 159.
(6) Andrew, E. R.; Bradbury, A.; Eades, R. G. *Nature* **1958**, *182*, 1659.
(7) Lowe, I. J. *Phys. Rev. Lett.* **1959**, *2*, 285.
(8) Wooten, E. W.; Muller, K. T.; Pines, A. *Acc. Chem. Res.* **1992**, *25*, 209.
(9) Chmelka, B. F.; Zwanziger, J. W. *NMR: Basic Principles and Progress.* **1994**, *33*, 79.
(10) Frydman, L. *Annu. Rev. Phys. Chem.* **2001**, *52*, 463.
(11) Gerstein, B. C.; Dybowski, C. *Transient Techniques in NMR of Solids: An Introduction to Theory and Practice*; Academic Press: Orlando, FL, 1985.
(12) Amoureux, J. P.; Fernandez, C.; Carpentier, L.; Cochon, E. *Phys. Status Solidi A* **1992**, *132*, 461.
(13) Gullion, T.; Schaefer, J. *Adv. Magn. Reson.* **1989**, *13*, 57.
(14) Griffiths, J. M.; Griffin, R. G. *Anal. Chim. Acta* **1993**, *283*, 1081.
(15) Schmidt-Rohr, K.; Spiess, H. W. *Multidimensional Solid-State NMR and Polymers*; Academic Press: London, 1994.
(16) Dusold, S.; Sebald, A. *Annu. Rep. NMR Spectrosc.* **2001**, *41*, 185.

10.1021/ja0214025 CCC: $25.00

proaches proposed to monitor dipolar couplings in powdered samples subject to MAS is the separated-local-field (SLF) experiment, a 2D NMR protocol which resolves for each chemically inequivalent site S in the sample its ^1H-S dipolar spinning sideband manifolds.[17−23] The purpose of the present study is to explore the consequences of applying a similar protocol to monitor heteronuclear local fields when S is a quadrupolar nucleus, that is, when monitoring the effects that nearby protons impose on the evolving central transitions of half-integer species being subject to MAS. Dipolar interactions can then be correlated with the second-order quadrupole patterns of the different species, leading to characteristic 2D intensity distributions between these two anisotropic NMR interactions that depend on the geometry and the dynamics of the particular H_n-S site. Adopting experimental approaches developed for the study of spin-$^1/_2$ powders, we explore in such fashion a variety of $^1H-^{11}B$ heteronuclear spin systems. Measurements repeated as a function of temperature reveal that, as was the case in spin-$^1/_2$ spectroscopy, SLF MAS NMR provides a sensitive route to the characterization of dynamics in quadrupole-containing solids. Finally, by incorporating into this experiment a high-resolution segment based on multiple-quantum MAS,[24] a 3D SLF NMR methodology enabling the characterization of these quadrupolar-dipolar MAS correlations in multisite systems is developed. Further borane examples of this new 3D NMR protocol, which has been recently introduced in brief in the literature,[25] are presented.

General Experimental and Theoretical Considerations

All the multidimensional NMR experiments described in this study were collected on laboratory-built spectrometers operating at 201, 302, and 501 MHz ^1H frequencies, equipped with 4 mm and 3.2 mm doubly tuned probes based on Varian/CMX Pencil spinning modules and capable of spinning samples up to 18 and 25 kHz, respectively. Radio frequency (rf) fields on the various irradiation channels had nutation frequencies in the order of 90 kHz, and TPPM decoupling schemes[26] were used during the data acquisition.

The various two-dimensional schemes employed throughout most SLF MAS NMR experiments discussed in this study are adaptations of similar methods employed for the study of spin-$^1/_2$ nuclei.[22,23] The basic sequence, illustrated in Figure 1A, correlates a purely heteronuclear dipolar evolution during time t_1 with a second-order quadrupolar anisotropy evolving during time t_2. Along the first, indirect dimension, sufficiently fast MAS rates are responsible for removing $^1H-^1H$ homonuclear dipolar couplings, while rotor-synchronized 180° pulses refocus the dephasing effects of the second-order quadrupolar anisotropy. Typical 2D acquisition experiments involved about 10 t_1 increments equally distributed over one rotational period T_r. The sideband spectra were obtained from the resulting dipole-encoded signals by renormalizing first the amplitude-modulated rotational echo at $t_1 = 0$ and $t_1 = T_r$; this amplitude-modulated single-period signal

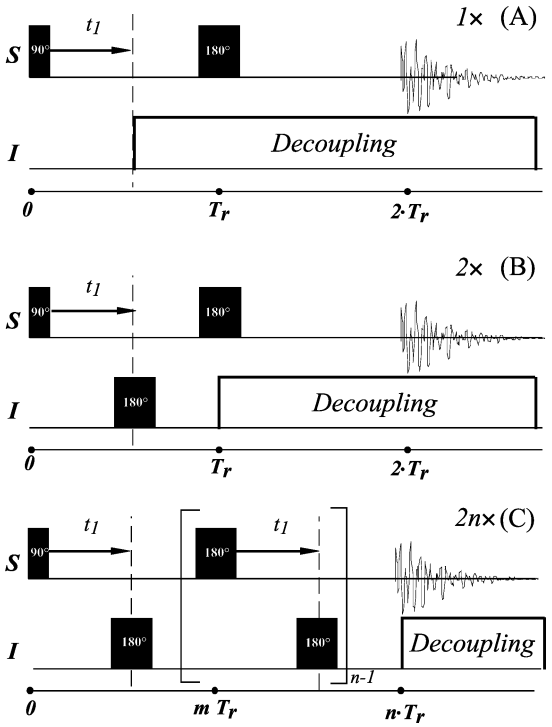

Figure 1. 2D SLF MAS NMR pulse sequences employed throughout the experiments discussed in this study. S denotes the half-integer quadrupolar species being detected; I the abundant spin-$^1/_2$ nucleus (usually ^1H) generating the local field; and T_r the duration of a rotational period (equal to the inverse of the MAS rate ν_r). (A) Basic 2D SLF scheme with second-order quadrupolar anisotropies being refocused during the time t_1 and no dipolar coupling amplification (*1*× experiment). (B) Same as part A but with a 2-fold amplification of the heteronuclear dipolar interaction. (C) Generic *2n*× pulse sequence with *2n*-amplified I−S dipolar evolution ($n = 2, 3, 4...$).

was then replicated until achieving the desired digital resolution along the indirect t_1 dimension and subject to Fourier transformation. Amplifying the apparent magnitudes of the ^1H-S dipolar interactions was also found often convenient or altogether necessary; this was achieved as described in refs 27 and 28, by inserting a series of rotor-synchronized 180° pulses in the t_1 evolution period (Figure 1B,C). These procedures, which we denote as *2n*× SLF experiments, give rise to MAS sideband patterns where either a *2n*-fold amplification in the dipolar coupling or, equivalently, an apparent *2n*-fold reduction in the MAS rate has taken place. Worth remarking about these *2n*× experiments is their constant-time nature, which usually makes the $t_1 = 0$, T_r renormalization procedure unnecessary.[29] This feature, combined with the time reversal associated with the MAS averaging process, also enabled us to characterize the dipolar t_1 dimension after monitoring only half a rotational period of SLF evolution.

Preliminary tests on the performance and self-consistency of these new techniques were carried out on the basis of numerical simulations focusing on $S-H_n$ multispin systems. A series of semiclassical 2D simulations focusing on an isolated $S-^1H$ spin pair where a heteronuclear dipolar MAS spectrum along the indirect dimension is correlated with a central-transition second-order quadrupolar MAS pattern along the directly detected dimension are presented in Figure 2. For the sake of simplicity, the MAS rate in these simulations was assumed small compared to the heteronuclear dipolar couplings yet larger than the span of the second-order MAS powder pattern. As evidenced by the spectral changes exhibited in this figure, patterns obtained in this manner

(17) Munowitz, M. G.; Griffin, R. G. *J. Chem. Phys.* **1982**, *76*, 2848.
(18) Munowitz, M. G.; Griffin, R. G.; Bodenhausen, G.; Wang, T. H. *J. Am. Chem. Soc.* **1981**, *103*, 2529.
(19) Schaefer, J.; McKay, R. A.; Stejskal, E. O.; Dixon, W. T. *J. Magn. Reson.* **1983**, *52*, 123.
(20) Schaefer, J.; Stejskal, E. O.; McKay, R. A.; Dixon, W. T. *Macromolecules* **1984**, *17*, 1479.
(21) Roberts, J. E.; Harbison, G. S.; Munowitz, M. G.; Herzfeld, J.; Griffin, R. G. *J. Am. Chem. Soc.* **1987**, *109*, 4163.
(22) Palmas, P.; Tekely, P.; Canet, D. *Solid State NMR* **1995**, *4*, 105.
(23) McElheny, D.; deVita, E.; Frydman, L. *J. Magn. Reson.* **2000**, *143*, 321.
(24) Frydman, L.; Harwood, J. S. *J. Am. Chem. Soc.* **1995**, *117*, 5367.
(25) Grinshtein, J.; Grant, C. V.; Frydman, L. *J. Am. Chem. Soc.* **2002**, *124*, 13344.
(26) Bennett, A. E.; Rienstra, C. M.; Auger, M.; Lakshmi, K. V.; Griffin, R. G. *J. Chem. Phys.* **1995**, *103*, 6951.
(27) Hong, M.; Gross, J. D.; Griffin, R. G. *J. Phys. Chem. B* **1997**, *101*, 5869.
(28) Hong, M.; Gross, J. D.; Rienstra, C. M.; Griffin, R. G.; Kumashiro, K. K.; Schmidt-Rohr, K. *J. Magn. Reson.* **1997**, *129*, 85.
(29) deVita, E.; Frydman, L. *J. Magn. Reson.* **2001**, *148*, 327.

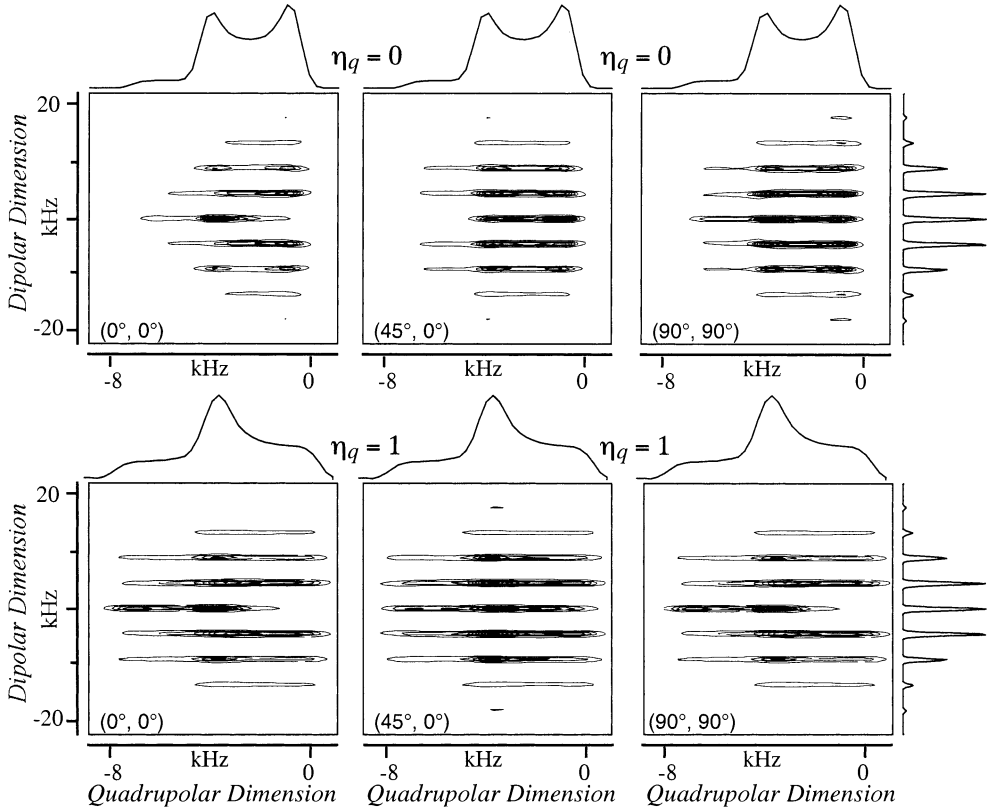

Figure 2. Simulated 2D SLF MAS NMR spectra expected for an isolated ^{1}H−S spin pair system as a function of the *(θ,φ)* Euler angles describing the orientation of S's dipolar and quadrupolar interaction tensors, computed for two different values of its quadrupolar asymmetry parameter η_q. Spectra were calculated for a MAS speed $\nu_r = 6$ kHz, assuming a strength of the ^{1}H−S dipolar interaction $\nu_d = 20$ kHz, quadrupolar coupling constant $C_q = 2$ MHz, and Larmor frequency $\nu_0 = 79.9$ MHz. In parallel to all *1*× experiments done in this work, these simulations focused on a single rotational period of dipolar evolution.

enable a retrieval of the quadrupolar and dipolar coupling parameters as well as an estimate on the mutual orientation relating the principal axes of these two coupling tensors. As we shall discuss later on, valuable dynamic insight is also conveyed by these 2D NMR line shapes.

In addition to this basic set of simulations, we compare in Figures 3 and 4 results that could be expected for prototypical I- -SI and SI_2 moieties from ideal sets of SLF MAS experiments involving solely quadrupolar and heteronuclear dipolar couplings effects, against the results that could be expected from experiments performed under the action of these as well as of homonuclear spin−spin couplings. The purpose of these simulations was to explore to what extent can expectations from semiclassical magnetization-vector simulations, applicable to isolated S−^{1}H pairs such as those assumed in Figure 2, be extrapolated to multispin systems containing ^{1}H−^{1}H couplings. To account for the latter, the full time propagation of SI_2 density matrixes was carried out over a single or over a few rotational periods (as demanded by the t_1 evolution) and over the full acquisition period under the sole action of quadrupolar effects. The resulting 2D data sets were then subject to the same type of postprocessing (renormalization, replication, weighting, Fourier transformation, and phasing) as was eventually applied on the experimental data sets. From the resulting patterns (Figures 3 and 4), we conclude that (i) quantitatively reliable data can be extracted from *2n*× SLF data for a bonded S−^{1}H system and (ii) semiquantitative conclusions can be extracted in such manner even for the more tightly coupled SH_2 groups. On invoking as well the simulations presented in Figure 2, we can also conclude that the dipolar patterns resulting from these SLF approaches can be employed to estimate the number of protons that are directly bonded to the quadrupolar site.

Results and Discussion

Structure and Dynamics of BH_n Groups ($n \leq 3$) Probed by 2D SLF MAS Techniques. ^{11}B, a spin-$^3/_2$ nucleus with a relatively high natural abundance, small quadrupole moment, and high Larmor frequency, was selected as a target to investigate the potential that 2D SLF MAS NMR experiments have to unravel structure and dynamics in solids. ^{11}B was chosen for this study due to its appearance in numerous different BH_n groups within boranes, a family of chemical compounds characterized by a variety of unusual properties that endow them in turn with unique potential applications.[30,31] These include roles as building blocks for nanoscale and structural devices, templates for catalysts, custom coordinating agents, and a variety of biomedical uses.[32−34] Most of these unique applications stem from boron's unusual bonding chemistry, second only to that of carbon in terms of its ability to establish multiple homo- as well as heteroatomic skeletons. Particular interest has been triggered over the decades by the distinct B−H motifs that can be found in boranes,[30] a topic which we decided to further inspect in the present study with the aid of the new SLF MAS technique. Generally, the B−H groups that were analyzed in the studied compounds (Scheme I) could be regarded as either of a "terminal" type, involving a pair of localized electrons contributed by a hydrogen orbital and by a hybridized boron orbital, or of a "bridging" type, where a pair of electrons is delocalized over a B−H−B three-atom center involving a hydrogen orbital and one hybrid orbital from each boron atom.

(30) Lipscomb, W. N. *Boron Hydrides*; Benjamin: New York, 1963.
(31) Grimes, R. N. ACS Symposium Series 827; American Chemical Society: Washington, DC, 2002; p 20.
(32) Casanova, J., Ed. *Borane, Carborane, Carbocation Continuum;* Wiley: New York, 1998.
(33) Greenwood, N. N. *Coord. Chem. Rev.* **2002**, *226*, 61.
(34) Ramachandran, P. V.; Brown, H. C. ACS Symposium Series 783; American Chemical Society: Washington, DC, 2001; p 1.

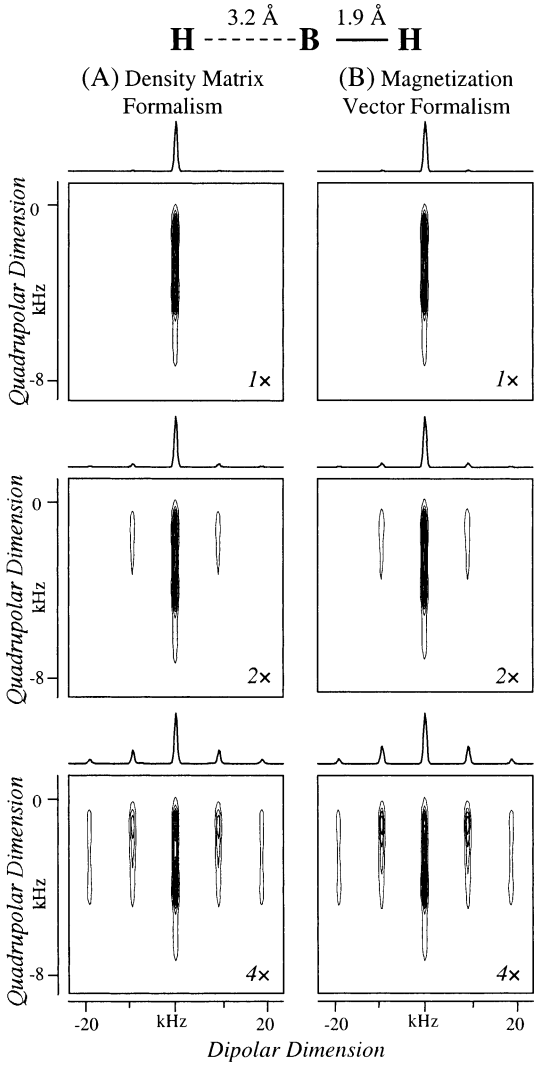

Figure 3. Quantum-mechanical (A) versus magnetization-vector-based (B) simulations of 2D SLF NMR spectra expected for an SI_2 system, using a prototypical ^{1}H--^{11}B^{1}H case as example. Spectra were calculated using the following parameters: $\nu_r = 10$ kHz, $C_q = 2.5$ MHz, $\eta_q = 0$, ν_d(H--B) = 1 kHz, ν_d(HB) = 5 kHz, $\nu_0 = 79.9$ MHz, and an arbitrary orientation between axially symmetric dipolar and quadrupolar tensors of 120°. The homonuclear ^{1}H−^{1}H dipolar coupling value incorporated in the density matrix simulations was 20 kHz.

Scheme 1

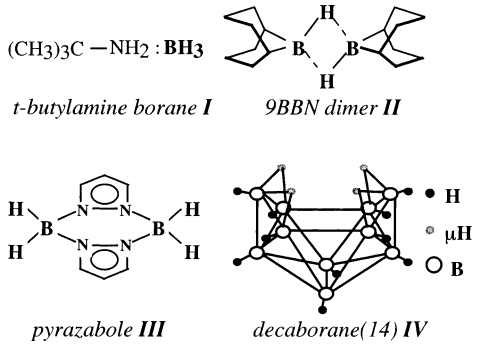

The left panel in Figure 5 shows a series of 2D SLF MAS NMR spectra for one such compound, *tert*-butylamine-borane **I**, involving a BH_3 with a normal type of bonding. Heteronuclear dipolar spinning sideband patterns appear in these plots along the horizontal dimension, correlated with the ^{11}B second-order quadrupolar line shape along the vertical one. An amplification

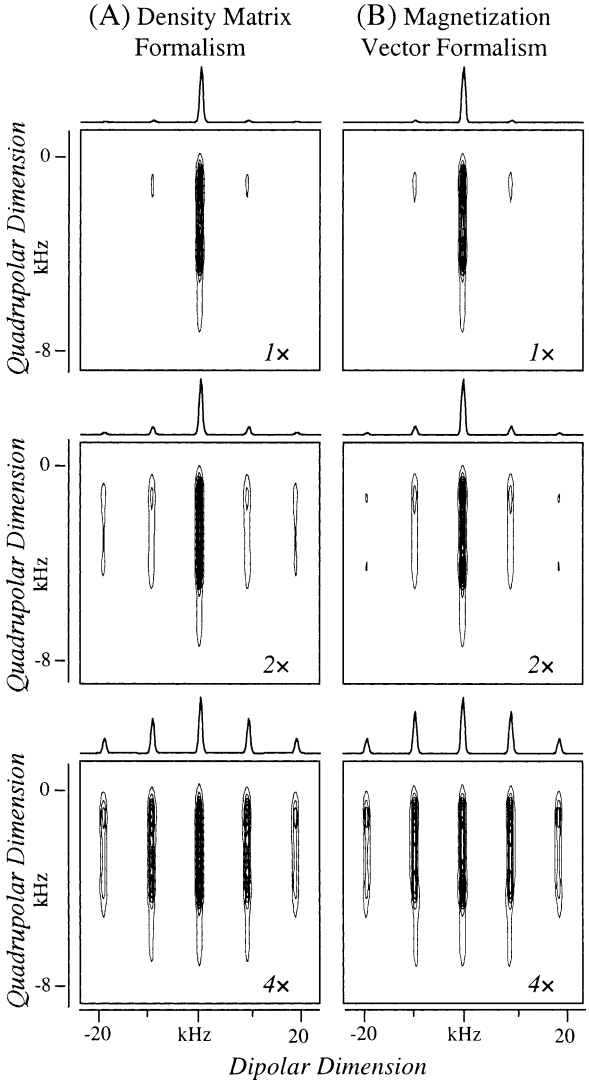

Figure 4. Idem as for Figure 3, but for a prototypical BH_2 system with a single ν_d(HB) dipolar coupling of 5 kHz.

of the apparent magnitudes of the heteronuclear dipolar interactions is evident upon employing the *2*× and *4*× SLF magnification routines. Dipolar coupling constants of ∼30 kHz could be expected from the typical ^{1}H−^{11}B bond distances arising in boranes, yet narrow dipolar sidebands patterns are observed in this group even at relatively slow spinning speeds and high amplification factors. This is diagnostic of the presence of dynamics. Indeed just as in methyl groups the presence of fast C_3-type motions will partially average out the intramoiety −CH_3 couplings, C_3 rotations of the borane along the B−N bond will make the ^{11}B quadrupole coupling tensor axially symmetric and partially average out ^{1}H−^{11}B dipolar spinning sidebands. The extent to which this averaging occurs can be used to gauge the angle subtended in these compounds by the N−B−H bond, as illustrated by simulations (Figure 5B) which incorporate a semiclassical magnetization-based model of a fast 3-fold rotation of the BH_3 group into their assumptions.

2D SLF MAS experiments were also carried out on boranes containing BH_2 groups in their structures. These dipolar measurements were implemented on the 9BBN dimer **II**, a borane for which high-resolution neutron diffraction shows a rigid four-center B−H_2−B structure with relatively short ^{11}B−

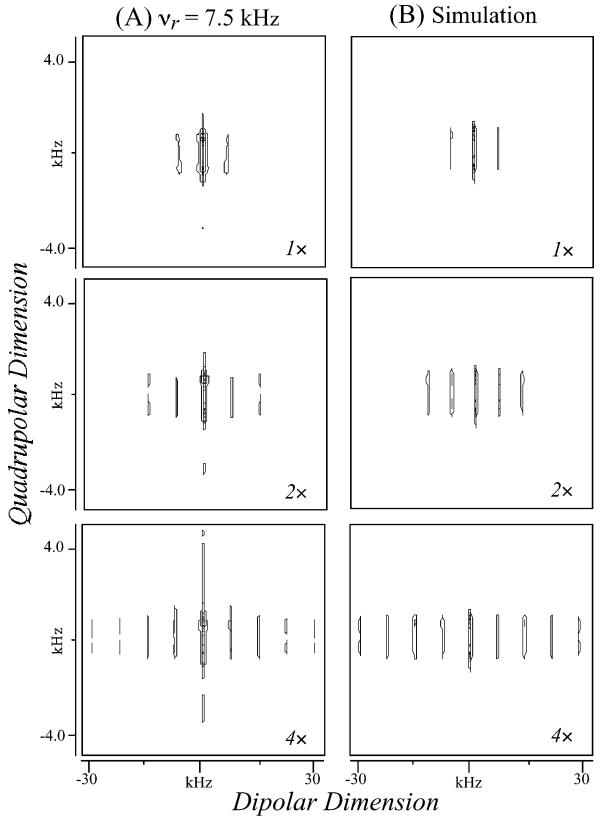

Figure 5. (A) Experimental 2D SLF MAS $n\times$ spectra acquired for *tert*-butylamine borane at 4.7 T using a 7.5 kHz MAS rate. (B) Magnetization-vector simulation of the experimental data set, based on a BH_3 group executing fast rotations around its C_3 symmetry axis where the N−B−H angle is 120°. Other fitting parameters: ν_d $(B-H)_{static}$ = 22 kHz, C_q = 1.61 MHz, η_q = 0.1.

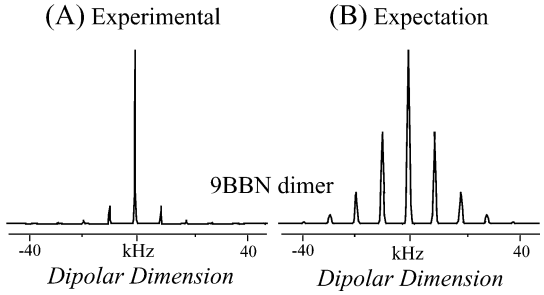

Figure 6. (A) ^{11}B SLF MAS NMR data recorded for the 9BBN dimer at a 10 kHz spinning speed and at room temperature. (B) Heteronuclear dipolar MAS sideband pattern expected for a BH_2 system based on the $\nu_d(B-H)$ = 19 kHz dipolar coupling derived from the compound's diffraction data.[35]

^1H bond distances.[35] Although a relatively intense SLF spinning sideband pattern was expected from this consideration for the boron atoms, only weak dipolar sidebands were observed along the BH_2's heteronuclear coupling domain (Figure 6A). Such experimental dipolar sideband patterns are in disagreement with what could be expected from static moieties (Figure 6B), and once again they are strongly suggestive of the occurrence of a fast dynamic process. One kind of dynamics which would be compatible with both these solid state NMR results and with the ordered structure observed via neutron diffraction consists of a hitherto uncharacterized mutual two-site exchange of the bridging hydrogens in this compound. To explore the potential effects of such local dynamics, the expected heteronuclear dipolar spectra within $-BH_2-$ groups were analyzed in simulations involving a mutual two-site exchange of the hydrogens in the spins' coupled Liouville space. Like the density matrix results described in the preceding paragraph, such simulations took into account both hetero- and homonuclear dipolar couplings under the action of MAS, as well as a mutual exchange dynamics that was formally accounted by the Alexander−Kaplan equation[36,37]

$$\frac{d\rho}{dt} = i[\rho,H] + k[R\rho R - \rho] \qquad (1)$$

where k is the rate of the hydrogens' reorientation and R is an exchange operator. This equation was rewritten in Liouville space in terms of exchange and Hamiltonian superoperators;[38] finding the time evolution of the $-BH_2-$ spin system then entailed solving a system composed by 64 coupled, time-dependent differential equations. Given the efforts involved in the explicit powder and time integration of such a Liouville-space problem, it seemed reasonable to check to what extent the homonuclear dipolar couplings that demand the use of this superoperator formalism actually affected the line shapes arising in SLF MAS NMR experiments. Therefore, a similar set of simulations was undertaken using a semiclassical formalism where the ^{11}B spin evolution was accounted by magnetization vectors and where $^1H-^1H$ interactions were altogether ignored. Dynamics could then be accounted for in these calculations by a simple McConnell-type modification of the SLF MAS Bloch equations.[2,39] Results arising from such dual semiclassical/quantum-mechanical sets of numerical simulations are compared in Figure 7. Two main conclusions can be drawn from these dipolar sidebands calculations. One stems from the similarity observed over the complete dynamic range between the predictions arising from both Liouville- and magnetization-space simulations. Such similarity indicates once again that, given the acquisition and processing conditions used in our experiments, it is justified to neglect homonuclear couplings and confine one's attention solely on local and heteronuclear dipolar interactions. The second main conclusion is that a fast, mutual hydrogen exchange process can indeed account for the substantial averaging observed in the dipolar sideband intensities observed in the BH_2 SLF MAS patterns of the 9BBN dimer.

To shed further light on the nature of this dynamic process, 2D SLF MAS NMR experiments on **II** were repeated as a function of temperatures. The expectation here was that, on lowering temperatures, line shape changes could be used to extract kinetic information about the rate of the hydrogen exchange. Though certain thermal changes could actually be discerned along the quadrupolar domain (Figure 8A), the dynamics of this process remained fast in the NMR time scale for the $^1H-^{11}B$ dipolar coupling dimension even at the lowest temperatures that we could reach (Figure 8B). Although no conclusive evidence is thus available about the process' kinetics, the rapid dynamics that we observe even at the lowest temperatures could be reflecting a tunneling process of the bridging hydrogens.

(35) Brauer, D. J.; Kruger, C. *Acta Crystallogr.* **1973**, *B29*, 1684.
(36) Alexander, S. *J. Chem. Phys.* **1962**, *37*, 967.
(37) Kaplan, J. *J. Chem. Phys.* **1958**, *29*, 462.
(38) Ernst, R. R.; Bodenhausen, G.; Wokaun, A. *Principles of Nuclear Magnetic Resonance in One and Two Dimensions*; Clarendon: Oxford, 1987.
(39) McConnell, H. M. *J. Chem. Phys.* **1958**, *28*, 430.

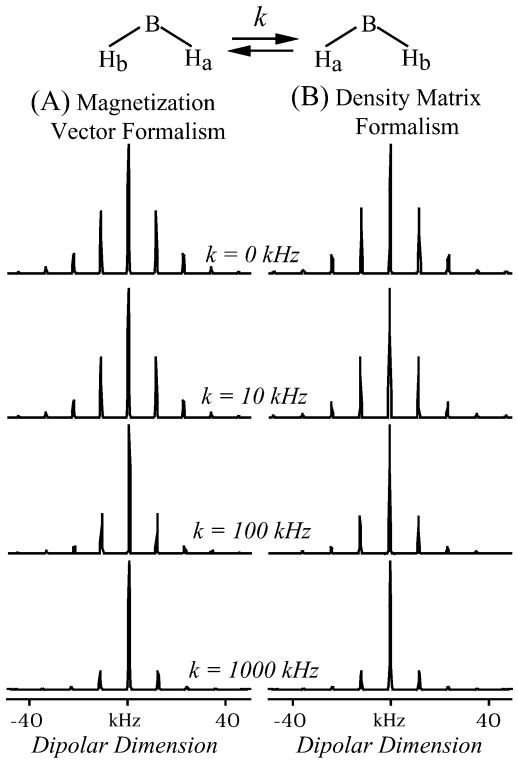

Figure 7. Dipolar sideband changes expected from a two-site chemical exchange process on a BH_2 group (akin to the one postulated for 9BBN), as this undergoes a two-site jump under MAS conditions. For both sets of simulations, spectra were calculated from the spins' evolution during half a rotational period assuming a 10 kHz spinning speed, a heteronuclear dipolar interaction strength of 19 kHz, and the indicated first-order kinetic rates *k* for the exchange process. The time-domain signal arising from these simulations was followed by the same replication/processing procedure as that used through the course of our SLF MAS NMR experiments. (A) Simulations resulting from a magnetization vector formalism where ^{1}H−^{1}H homonuclear couplings are neglected. (B) Simulations resulting upon using the exchange superoperator formalism, and including a 24 kHz ^{1}H−^{1}H homonuclear dipolar coupling. In both cases, the tensors' transformations leading from the PAS of an internuclear dipolar vector to the main magnetic field were assembled as PAS $\xrightarrow{(0°,\ \pm\beta/2,\ 0°)}$ Molecule $\xrightarrow{(\phi,\ \theta,\ 0°)}$ Rotor $\xrightarrow{(\nu_r t,\ 54.7°,\ 0°)}$ Lab. The H−B−H angle β was set to 86°, according to 9BBN's diffraction structure.[35]

Another BH_2-containing compound analyzed by this methodology was pyrazabole (Scheme 1, **III**). X-ray analyses have revealed the potential presence of two conformations for this compound, a "boat" one and a "chair" one, with the former being stable at room temperature and the latter becoming favored at higher temperatures.[40] Figure 9 shows a variable-temperature set of 1D ^{11}B MAS NMR spectra for this compound in the solid phase, where one can appreciate that on exceeding 50 °C a second resonance does indeed start appearing, even if the full extent of these changes becomes truncated by the relatively low melting point of the powder (80 °C). Changes upon increasing the temperature of this powder are also evidenced by the 2D SLF MAS ^{11}B NMR data summarized in Figure 10, which reveal that whereas a static-like dipolar sideband pattern characterizes the conformation that is stable at room temperature, a much more mobile population (weaker effective dipolar interactions) appears upon heating. It thus appears that the lower-temperature form, which for the sake of consistency with the

(40) Niedzu, K. *Mol. Struct. Energ.* **1988**, *5*, 357.

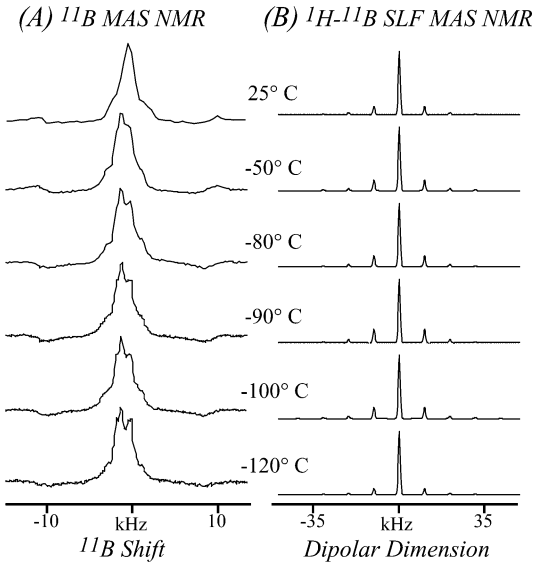

Figure 8. Variable-temperature ^{11}B NMR data acquired for the 9BBN dimer at 7.2 T with a MAS rate ν_r = 10 kHz. (A) ^{1}H-decoupled 1D MAS ^{11}B spectrum. (B) Dipolar sideband patterns extracted from 2D SLF MAS ^{11}B NMR experiments.

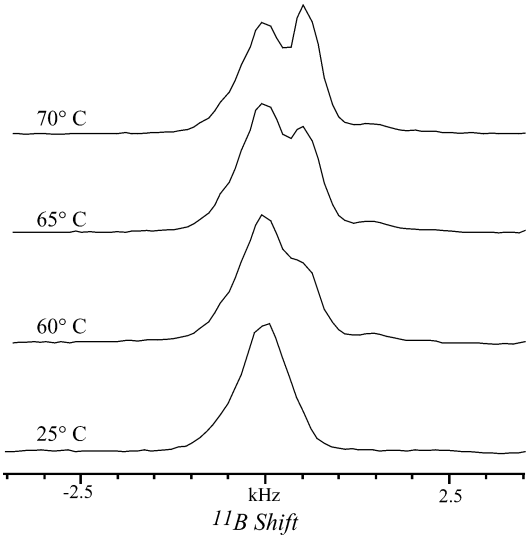

Figure 9. Variable-temperature ^{11}B MAS NMR data acquired for a pyrazabole sample spinning at ν_r = 10 kHz (11.7 T), while using ^{1}H-decoupling.

X-ray data we shall refer to as the "boat" form, is characteristic of a static BH_2-like structure, whereas the "chair" conformation that appears on heating exhibits averaged SLF patterns that resemble those arising from the fast two-site exchange dynamics illustrated in Figure 7. Although it is tempting to invoke a mutual hydrogen exchange dynamics as well for pyrazabole, it should be noted that this resemblance might be circumstantial, as it is apparent that in unison with the fast motion of the hydrogens a more extensive kind of molecular motion is present. This is evidenced by the collapse of the ^{11}B quadrupole coupling parameters in the high-temperature form, suggesting the presence of a "chair"-to-"chair" reorganization or a 2-fold rotation of the molecules as a whole in the solid.

The SLF MAS examples described so far were mainly concerned with applications to relatively simple compounds, involving a single or at most two types of boron sites. Unlike these cases, the final compound to be discussed, *nido*-decabo-

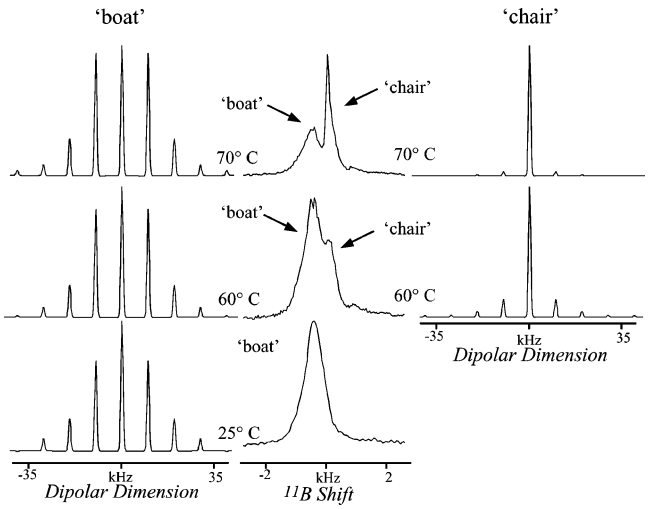

Figure 10. Variable-temperature 2D SLF MAS NMR data collected for a pyrazabole sample (11.7 T) with $\nu_r = 10$ kHz. The dipolar slices extracted for the indicated peaks correspond to boat and chair conformations, as judging from X-ray evidence and from their dynamic behavior.

rane(14) (Scheme I, **IV**), comprises several inequivalent borons. This molecule exhibits an overall C_{2v} symmetry and has four different types of boron atoms; its classification in accordance with the STYX rule can be estimated as 4620, with S and T denoting the number of three-center two-electron B−H−B and B−B−B bonds and X and Y standing for the number of normal two-center two-electron B−H and B−B bonds.[30] Even if potential structural subtleties in this nonclassical chemical system are kept in mind, it is convenient to reclassify this borane's ^{11}B environments according to a conventional BH_n discrimination, as eventually it will be this type of information that SLF MAS NMR will monitor. Henceforth, we catalog the various atomic sites in the decaborane molecule as comprising four BH spin pairs (B1, B2, B3, B4), four BH_2 groups (B5, B7, B8, B10), and two BH_3 moieties (B6 and B9). The chemical nature of these decaborane sites, together with one-dimensional ^{11}B NMR spectra acquired for the compound in solid and liquid phases, are presented in Figure 11. Whereas the four chemically inequivalent sites present in the borane can be clearly distinguished by liquid state ^{11}B NMR (Figure 11A), homonuclear dipolar and second-order quadrupolar broadenings coupled to apparent shifts of the various resonances conspire into making the MAS spectrum of the solid powder poorly resolved (Figure 11B). Still, on the basis of the solution-phase ^{11}B assignments,[41] the three peaks appearing in the MAS spectrum could be ascribed to superpositions of B1, B3 ("BH"), B6, and B9 ("BH_3"), all falling into peak **a**, of B10, B8, B5, and B7 ("BH_2") comprising peak **b**, and of B2 and B4 ("BH") appearing in peak **c** of the solids NMR trace.

Homonuclear ^{11}B−^{11}B dipolar couplings are particularly relevant to solid NMR experiments on decaborane, as they result in substantial line broadening effects unless fairly fast (>10 kHz) MAS rates are employed. Even then they result in severe signal losses when spin−echoes are attempted on the boron channel, a feature that forced us to circumvent the use of 180° pulses for refocusing second-order quadrupole and chemical shift effects in the SLF MAS experiments. Instead, we relied on

(41) Clouse, A. O.; Moody, D. C.; Rietz, R. R.; Rospberry, T.; Schaeffer, R. *J. Am. Chem. Soc.* **1973**, *95*, 2496.

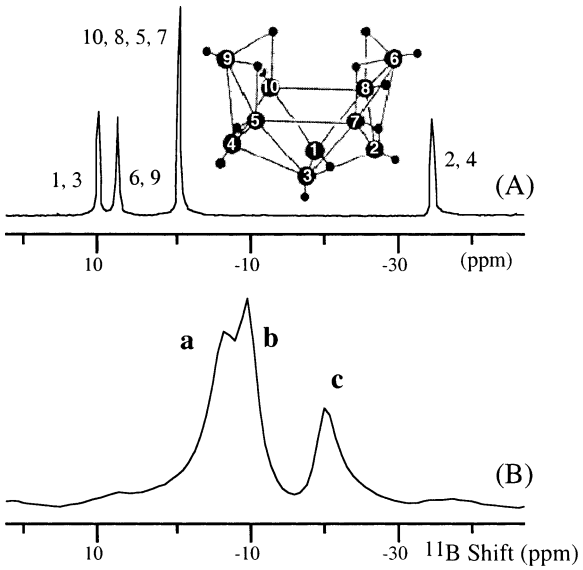

Figure 11. ^{11}B NMR spectra of decaborane recorded at 11.7 T. (A) Solution trace recorded in *n*-hexane with ^{1}H decoupling, showing the literature-based assignment of the peaks. (B) Solid state ^{1}H-decoupled MAS spectrum acquired on the powder at a $\nu_r = 15$ kHz spinning speed.

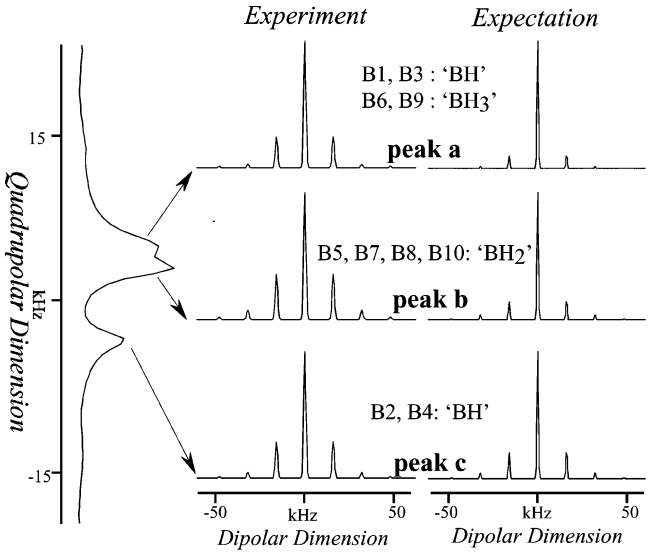

Figure 12. Summary of the 2D SLF data recorded for decaborane at 11.7 T and $\nu_r = 15$ kHz MAS rate. Notice the discrepancies in both absolute and relative sideband intensities arising between the partially resolved experimental ^{11}B MAS dipolar manifolds and the expectation based on the indicated solution-state peak assignment.

shearing transformations in order to remove these single-spin ^{11}B-based contributions occurring during the time t_1. 2D SLF MAS results collected in this fashion for the compound are summarized in Figure 12. Although a lack in resolution in these 2D data complicates their analysis, dipolar slices can be extracted for the three main ^{11}B peaks given by the molecule. It becomes clear then that the dipolar patterns arising from these experiments do not match the trend that is to be expected from the peak's assignment taken from the liquid state spectrum. Indeed, the peaks labeled **a** and **c** appear with almost identical dipolar sideband intensities, whereas the previously mentioned assignment predicts a stronger nondynamic "BH_3"-like spinning sideband pattern dominating the former (due to the contributions of B6 and B9) and a weaker "BH"-type sideband pattern (from B2 and B4) dominating the latter.

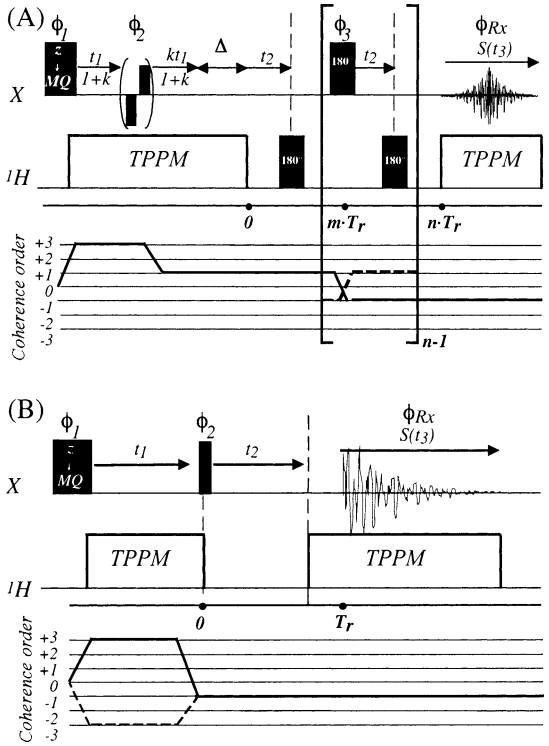

Figure 13. 3D MQMAS-based pulse sequences proposed for the acquisition of isotropically resolved SLF sideband patterns. (A) Generic 3D scheme employed for *2n*-amplified effective ^{1}H−X local fields, in combination with an FAM-based MQMAS sequence.[47,48] (B) Simplified 3D MQSLF MAS scheme restricting the use of 180° pulses and employed on the decaborane sample. Data corresponding to echo and antiecho pathways, indicated by dashed and full lines, respectively, were collected in this sequence on independent acquisitions.

Three-Dimensional High-Resolution Local-Field Techniques: Decaborane Analysis. Decaborane represents a common example among compounds that might become a target of SLF MAS experiments, in the sense that like most of these it contains several inequivalent sites in the molecule or in the crystal cell. However, as MAS is by itself unable to remove the anisotropies originating from second-order quadrupole effects, the 2D SLF versions described in the preceding paragraphs will in general be unable to resolve all inequivalent sites along the direct acquisition dimension. This lack of resolution along with the decaborane ambiguities mentioned previously prompted us to combine the 2D SLF protocol with multiple-quantum MAS (MQMAS[24]) in an effort to improve spectral resolution among the inequivalent chemical sites. We have actually discussed recently the incorporation of MQMAS into the SLF experiment for the sake of achieving such site resolution and illustrated its potential on a series of mononucleotidic sodium salts;[25] this last paragraph is devoted to a deeper explanation of this experiment and how it was modified to help unravel the decaborane SLF results.

Figure 13 shows two versions of pulse sequences that combine SLF with MQMAS routines. Part A illustrates the kind of pulse sequence assayed in ref 25, where the isotropic evolution portion of a split-t_1 MQMAS NMR experiment[42,43] is merged with 2D SLF experiments of the kind introduced in Figure 1. The initial part of this sequence involves multiple- and single-quantum evolution periods chosen according to the MQMAS rules for isotropic refocusing: $^9/_{16}t_1$ and $^7/_{16}t_1$ evolution fractions for the spin-$^3/_2$ nucleus here under consideration. This isotropic phase encoding $\exp[i\nu_{iso}t_1]$ is followed by a constant-time delay $\Delta = nT_r$ whose goal is to eventually lead to the formation of an echo along the directly detected dimension, by a ^{1}H-coupled evolution period t_2 encoding in an amplitude-modulated fashion of the dipolar MAS evolution frequency $\nu_{dip}(t')$, and by a final t_3 detection period monitoring the central-transition frequency ν_{CT}. Neglecting the minor time dependencies introduced by MAS on the shielding and quadrupolar evolution frequencies, we can summarize the resulting signal as

$$S(t_1,t_2,t_3) = \int\int\int I(\nu_{iso},\nu_{dip},\nu_{CT}) \exp[i\nu_{iso}t_1] \cos[\int_0^{t_2} \nu_{dip}(t')dt'] \exp[i\nu_{CT}(t_3 - \Delta)]\, d\nu_{iso}\, d\nu_{dip}\, d\nu_{CT} \quad (2)$$

As this signal involves the formation of an echo at the center of the acquisition period t_3 for all t_1 values as well as an amplitude modulation along the t_2 dimension, it allows one to calculate purely absorptive peak shapes from a single 3D NMR experiment. From this standpoint, this makes such a version of the 3D MQMAS SLF sequences the most convenient among those we have assayed on routine assignment applications.

Unfortunately we found that, due to the presence of the extensive network of coupled ^{11}B homonuclei, such a pulse sequence was not an effective route to the analysis of decaborane. As mentioned, this system suffers severe signal losses when studied using sequences based on 180° pulses and relatively long echo delays, of which Figure 13A has several. Instead, the simpler alternative in Figure 13B was thus chosen to investigate $B_{10}H_{14}$; this incorporates a phase-modulated evolution time t_1 under the action of multiple-quantum ν_{MQ} frequencies, a dipole-coupled 1Q evolution period t_2, and a final central-transition evolution during the acquisition time t_3. The signal thus available from this 3D sequence is

$$S(t_1,t_2,t_3) = \int\int\int I(\nu_{MQ},\nu_{dip},\nu_{CT})\exp[i\nu_{MQ}t_1]\exp[i\nu_{CT}t_2] \cos[\int_0^{t_2} \nu_{dip}(t')dt']\exp[i\nu_{CT}t_3]\, d\nu_{MQ}\, d\nu_{dip}\, d\nu_{CT} \quad (3)$$

Unlike the previous 3D sequence, this approach requires collecting data arising from both echo and antiecho pathways along the MQ evolution domain for obtaining purely absorptive line shapes, as well as an optional shearing of the data within the SLF plane to retrieve purely dipolar and central-transition evolution frequencies.

Figure 14 summarizes representative ^{11}B NMR results that were observed with this latter pulse sequence on decaborane. Even a superficial comparison reveals a substantial resolution enhancement upon going from 1D MAS to 2D MQMAS spectra. Furthermore, the MQMAS spectrum enables a model-free analysis of the sites' shielding and quadrupolar coupling parameters from the centers of mass of the various peaks.[44,45] Such analysis is key in the interpretation of the decaborane data, as it indicates that considerable changes in the isotropic chemical shifts of the sites occur upon taking the molecule from the liquid

(42) Brown, S. P.; Wimperis, S. *J. Magn. Reson.* **1997**, *124*, 279.
(43) Brown, S. P.; Heyes, S. J.; Wimperis, S. *J. Magn. Reson.* **1996**, *A119*, 280.
(44) Medek, A.; Harwood, J. S.; Frydman, L. *J. Am. Chem. Soc.* **1995**, *117*, 12779.
(45) Milliot, Y.; Man, P. P. *Solid State NMR* **2002**, *21*, 21.

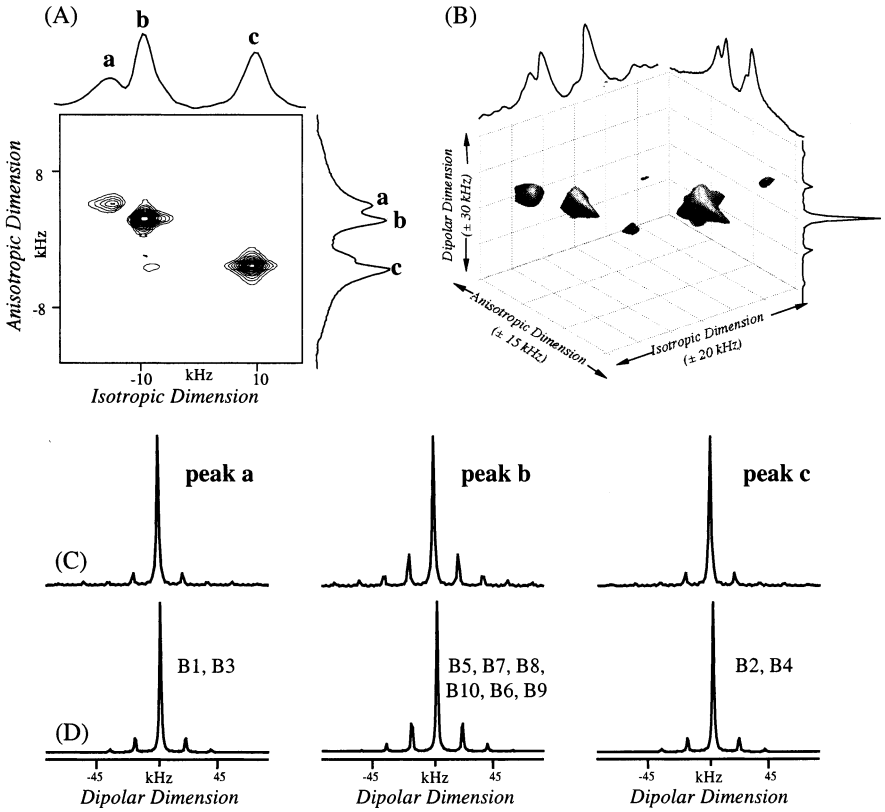

Figure 14. (A) 2D MQMAS spectrum of decaborane recorded at 15.8 kHz MAS rate and 11.7 T. (B) Isosurface representation of a fully processed 3D MQMAS SLF ^{11}B NMR spectrum recorded under similar conditions for decaborane, utilizing the pulse sequence shown in Figure 13B and processed as described in the text. (C) Array of 1D dipolar slices resolved from the 3D spectrum. (D) Simulations of the dipolar patterns in part C calculated on the basis of ^{11}B−^{1}H distances available from X-ray diffraction and of the site assignment illustrated for each trace.

Table 1. Parameters Identified for Various Boron Sites in Decaborane(14)

^{11}B site	δ^{cs} solids[a] (liquids)[b]	C_q (MHz)[a]	R(B–H$_t$)[c]	(θ, ϕ)[a]
1, 3 (BH)	9 (12.2)	1.7	1.28	0°, 0°
2, 4 (BH)	−33 (−36.5)	1.4	1.29	0°, 0°
5, 10 (BH_2)	−3 (0.2)	1.3	1.29, 1.34	150°, 0°
7, 8 (BH_2)	−3 (0.2)	1.3	1.26, 1.34	150°, 0°
6, 9 (BH_3)	−3 (9.5)	1.3	1.25, 1.40, 1.40	108°, 0°

[a] Values extracted from fitting the 2D MQMAS and 3D MQMAS/SLF NMR data. [b] Chemical shifts expressed in parts per million with respect to neat $B(OCH_3)_3$. [c] Distances according to the diffraction data in ref 46.

to the solid phase. This in turn provides a clue regarding the discrepancies arising between the expected ^{1}H−^{11}B SLF patterns and those revealed by the experiments, as it suggests that sites have shifted in the solid from their solution state progression. A proper explanation for the different dipolar strengths exhibited by the various ^{11}B MAS NMR peaks can then result if it is assumed that the "BH_3-type" boron atoms B6 and B9, initially presumed to overlap with the "BH"-types B1 and B3 in the solid spectrum, have moved from peak **a** into the nearby resonance **b**. This shift of the most strongly dipole-coupled sites from the edge to the center of the spectrum will then decrease the dipolar sidebands expected from peak **a** while increasing those expected from peak **b**. Under these assumptions, summarized in Table 1, the dipolar MAS slices extracted for the various sites from the three-dimensional data set match very well the SLF simulations that can be expected for each peak on the basis of the ^{1}H−^{11}B distances reported by the X-ray diffraction data (Figure 14D).[46]

Conclusions

The present work explored both theoretically and experimentally the potential arising when extending separated-local-field techniques to the study of half-integer quadrupole nuclei. Such NMR techniques are well-established in the area of spin-$^1/_2$ spectroscopy, yet are only beginning to be explored for higher spin numbers. As illustrated throughout the paper, furthering such experiments may provide a wealth of information concerning different aspects affecting quadrupolar sites in solids, particularly in terms of assigning the chemical environments surrounding such nuclei, which are often much more varied than those characterizing their spin-$^1/_2$ counterparts, and in terms of the valuable dynamic insight that these methods can reveal.

In terms of their execution, the SLF experiments that were here described are relatively simple: they do not demand the use of complex pulse sequences, they are characterized by competitive signal-to-noise ratios when compared to standard MAS, and by requiring few increments along the dipolar-encoding dimension, they end up being relatively short. Indeed the fact that the experiment can be focused on measuring just a few dipolar evolution points within a single rotational period, or in many cases even within half a period alone, endows it with the possibility of achieving high *S*/*N* in short acquisition times. It is mainly thanks to this feature that the experiment's eventual extension into a high-resolution 3D NMR format in

(46) Kasper, J. S.; Lucht, C. M.; Harker, D. *Acta Crystallogr.* **1950**, *3*, 436.
(47) Madhu, P. K.; Goldbourt, A.; Frydman, L.; Vega, S. *Chem. Phys. Lett.* **1999**, *307*, 41.
(48) Madhu, P. K.; Goldbourt, A.; Frydman, L.; Vega, S. *J. Chem. Phys.* **2000**, *112*, 2377.

combination with the relatively insensitive MQMAS technique becomes feasible. All these features also enable the repetitive performance of SLF measurements as a function of temperatures, therefore making this method a suitable probe of molecular dynamics.

Dynamics was the one main feature observed in a majority of the compounds that were analyzed. This is remarkable because our attention centered on a thoroughly studied series of borane compounds, for which previous X-ray and neutron diffraction studies had suggested static structures. It is thus likely that systematic applications of this and of other half-integer quadrupolar NMR dynamic methods might reveal about inorganic and bioinorganic solids, a motional picture akin to that which ^{2}H and spin-$^{1}/_{2}$ NMR revealed over the last few decades for the case of several organic systems. This hypothesis is currently under exploration.

Acknowledgment. This work was supported by the Philip M. Klutznick Fund for Research (Weizmann Institute) and by the Israeli Science Foundation (Grant # 296/01).

JA0214025